remote sensing

MDPI

Article

A Multi-Satellite Space Environment Risk Prediction and Real-Time Warning System for Satellite Safety Management

Ning Kang [1,2], Liguo Zhang [3], Weiguo Zong [1,2], Pan Huang [4,5], Yuqiang Zhang [6], Chen Zhou [6], Jian Qiao [7] and Bingsen Xue [1,2,*]

1 Key Laboratory of Space Weather, National Satellite Meteorological Center (National Center for Space Weather), China Meteorological Administration, Beijing 100081, China; kangn@cma.gov.cn (N.K.); zongwg@cma.gov.cn (W.Z.)
2 Innovation Center for FengYun Meteorological Satellite (FYSIC), Beijing 100081, China
3 Shanghai Institute of Satellite Engineering, Shanghai 201109, China; 201621480057@mail.bnu.edu.cn
4 Department of Aerospace Information Engineering (Image Processing Center), School of Astronautics, Beihang University, Beijing 102206, China; by2315144@buaa.edu.cn
5 CASIC Research Institute of Intelligent Decision Engineering, Wuhan 430040, China
6 Department of Space Physics, School of Electronic Information, Wuhan University, Wuhan 430072, China; yqzhang@whu.edu.cn (Y.Z.); chenzhou@whu.edu.cn (C.Z.)
7 Key Laboratory of Environmental Change and Natural Disaster, Ministry of Education, Beijing Normal University, Beijing 100875, China; qiaojian@picc.com.cn
* Correspondence: xuebs@cma.gov.cn

Abstract: In response to the need for a space security situation assessment during orbit, the multi-satellite space environmental risk prediction and early warning system is based on the detection results of the space weather payload of the Fengyun 4A and 4B satellites, as well as the prediction results of the National Space Weather Center, for the first time. By comprehensively utilizing some open-source data, it is the first time that we have achieved a 24 h advanced prediction of the space environment high-energy proton, low-energy particle, and high-energy electron risks for the safety of the Fengyun-series high-orbit satellites, and a real-time warning of satellite single-event upset, surface charging, and deep charging risks. The automation system has preliminarily achieved an intelligent space risk assessment for the safety of multiple stationary meteorological satellites, effectively improving the application efficiency of the space environmental data and the products of Fengyun-series satellites. The business status is stable in operation, and the resulting error between the predicted results of various risk indices and the measured data was less than one level. The warning accuracy was better than 90%. This article uses the system for the first time, to use Fengyun satellite data to, accurately and in a timely manner, predict and warn us about the low-energy particles and surface charging high-risk levels of the Fengyun 4A and 4B satellites during the typical space weather event on 21 April 2023, in response to the impact of complex spatial environmental factors on the safety of Fengyun-series high-orbit satellites. The construction and operation of a multi-satellite space environmental risk prediction and early warning system can provide a reference for the safety work of subsequent satellite ground system operations.

Keywords: satellite security; space environment; risk prediction; real-time warning

check for updates

Citation: Kang, N.; Zhang, L.; Zong, W.; Huang, P.; Zhang, Y.; Zhou, C.; Qiao, J.; Xue, B. A Multi-Satellite Space Environment Risk Prediction and Real-Time Warning System for Satellite Safety Management. *Remote Sens.* **2024**, *16*, 1814. https://doi.org/10.3390/rs16101814

Academic Editor: Xiaogong Hu

Received: 30 January 2024
Revised: 30 April 2024
Accepted: 12 May 2024
Published: 20 May 2024

Copyright: © 2024 by the authors. Licensee MDPI, Basel, Switzerland. This article is an open access article distributed under the terms and conditions of the Creative Commons Attribution (CC BY) license (https://creativecommons.org/licenses/by/4.0/).

1. Introduction

With the development of space technology, satellites flying in space are becoming increasingly complex. In the absence of atmospheric protection, the complex space weather environment is very prone to affecting the satellite payload, endangering satellite safety and normal operation. There are many international and domestic satellites carrying space weather monitoring payloads [1–4]; among these, the NASA Global-scale Observations of the Limb and Disk (GOLD) mission has flown an ultraviolet-imaging spectrograph on

SES-14, which uses two identical channels to observe Earth's far-ultraviolet (FUV) airglow at a distance of ~134–162 nm [5]. The Swarm mission of the European Space Agency's Earth Exploration Program (ESA) uses three satellites in a lower altitude, two of which measure the gradient of the magnetic field. The measured magnetic field is the sum of many contributions including the magnetic fields and currents inside the Earth, as well as the currents in Earth's space [6]. The FY-4 series is China's new-generation geosynchronous-orbit meteorological satellite. Currently in orbit, it includes Fengyun-4A (hereinafter referred to as FY-4A) and Fengyun-4B (hereinafter referred to as FY-4B). The space weather instruments carried by FY-4A include high-energy electron detectors, high-energy proton detectors, fluxgate magnetometers, and radiation dosimeters, respectively. The FY-4B space weather instrument is composed of a charging potential monitor, on the basis of inheriting the high-energy charged particles and space magnetic field detection capabilities of the FY-4A satellite space weather monitoring instrument package. It has the same ability to detect high-energy charged particles and space magnetic fields, and can detect the medium-energy charged particles, low-energy charged particles, multi-band ionospheric ultraviolet spectral image, solar polar ultraviolet image, and X-EUV flow. Double satellites conducting space exploration simultaneously in high orbit can greatly enhance the space weather operation capabilities, provide guarantees for space weather users such as the aerospace industry, adapt to the development of national space weather monitoring and warning products, enhance national space weather monitoring, warning, and service capabilities, provide space weather monitoring and warning products with independent monitoring data for the public and professional users, and improve China's space weather monitoring, warning, and service capabilities [7,8]. The FY4-(02) batch ground application system serves as the full business process support system for the FY-4B satellite, which is divided into ten major systems according to function, including the Space Weather Application System (SWAS) and Mission Management & Control System (MCS) [9,10]. Among them, the SWAS uploads the status information of space weather products and subsystems at all levels to the MCS, and the MCS s is responsible for the integrated safety management and scheduling control of satellite and ground application systems [11–13].

With the increasing number of Fengyun-series meteorological satellites in orbit, the probability of various types of payload devices being affected by space weather continues to increase. The high timeliness and reliability requirements for space weather forecasting and the early warning for satellite safety pose a challenge to the existing satellite safety and health management system. Many studies have been conducted on the impact of space weather factors on satellite safety and protective measures. Robin and John found that surface charging and deep dielectric charging are two common causes of satellite anomalies [14]; Randall et al. found that high-energy particle precipitation during solar storms leads to the production of a large amount of nitrogen oxides in the upper atmosphere [15]; Rozanov et al. found that the response amplitude of the atmosphere to high-energy electron precipitation events may exceed the influence of solar ultraviolet flux [16]; Fennell et al. found that, when the differential potential value is large and negative, it usually occurs at night, and the number of occurrences during the day is less than 1% [17]. The high-energy protons from progressive solar high-energy particle events may pose significant radiation hazards to astronauts, space equipment, and high-altitude aircraft passengers flying polar routes [18]. W. DRGE et al. analyzed the 65–105 keV electrons observed in a solar electron event observed by STEREO-A, STEREO-B, and ACE, and proposed, based on a three-dimensional particle propagation model, that, in the energy range of approximately 60–300 keV, due to the non-radial divergence of magnetic field lines or particle diffusion, the lateral transmission of electrons partially occurs near the sun and partially occurs in the interstellar medium [19]. Verkhogliadova et al. used the Monte Carlo method to model the transport of particles escaping from impact, obtained the time intensity distribution of protons and iron ions, and analyzed the radial correlation of the peak flux (J) of protons and iron ions from 0.5 to 2AU [20]. Wang et al. studied the occurrence time of solar high-energy particle events through numerical simulation, using a three-dimensional focused

transport model to calculate the proton flux observed in the ecliptic at 1 AU in the energy range between 10 MeV and 80 MeV, confirming that the VDA method is effective for the pulse source duration, low background, weak scattering in interplanetary space, or rapid diffusion in the solar atmosphere [21].

China is still in the exploratory stage of predicting and warning us about the space environment index for satellite safety [22,23]. During the construction period of the MCS, in order to meet the risk prediction and real-time warning requirements for the impact of space weather factors on satellite safety [24,25], based on the SWAS subsystem space weather data, the space weather payload detection results of the FY-4A and FY-4B are used for the first time and the National Center for Space Weather (NCSW) prediction results, combined with some open-source data, are designed to predict the comprehensive risk index of multi-star high-energy protons, low-energy particles, and high-energy electrons, as well as real-time risk index warnings for multi-satellite SEU, surface charging, and deep charging. Furthermore, through the deployment of a full-process multi-satellite space environment risk prediction and real-time warning automation system in the MCS subsystem, a commercial 24 h prediction and real-time warning service for the safety of Fengyun-series high-orbit satellites is achieved for the first time, improving the timeliness, stability, and reliability of satellite safety space environment assessment automation.

2. Data and Methods

The multi-satellite space environmental risk prediction and real-time warning system mainly uses independent data sources from FY-4A and FY-4B satellites, provided by the National Space Weather Monitoring and Warning Center [26]. Through the Fengyun-4 ground application system business operation platform, it can continuously and stably obtain all the data required for forecasting and warning level division functions. Part of the open-source data used is provided by the Space Weather Prediction Center (SWPC) and the World Data Center for Geomagnetism (WDC Kyoto) at Kyoto University in Japan, which can effectively improve the time accuracy of risk forecasting.

The Fengyun-4 meteorological satellite space weather business system constructed by NCSW is based on real-time and continuous monitoring of near-Earth space environment data by FY-4A and FY-4B satellites, achieving the full business process of space weather monitoring, data preprocessing, product generation, storage, and distribution, and, through a complete service system that includes service product generation, product application, and evaluation, it meets the different needs of decision-making for the public and the professional users [27]. Space Weather Prediction Center (SWPC) is a laboratory and weather forecasting center of the National Oceanic and Atmospheric Administration (NOAA) of the United States [28]; its website (https://www.swpc.noaa.gov/, accessed on 7 May 2023) updates 1-day data every 5 min, including electron flux, geomagnetic index, proton flux X-ray flux, planetary K-index, real-time solar wind, and K-station and A-station indices. At the same time, the website can provide a 27-day outlook for 3-day geomagnetic forecasts, sunspot numbers, solar cycles, 10.7 cm radio flux, and geomagnetic indices, with proton event probability data and the high-energy proton Fp index, the solar wind, and Ap index data. World Data Center for Geomagnetism, Kyoto, Japan (https://wdc.kugi.kyoto-u.ac.jp, accessed on 8 May 2023) provides geomagnetic field data on its official website, including AE index, ASY/SYM index, and Dst index [29]. The introduction of automatic data acquisition by the multi-satellite space environmental risk prediction and real-time warning system is shown in Table 1.

The design of a multi-satellite space environment risk prediction and real-time warning system focuses on various factors that affect satellite safety and space weather. The comprehensive risk prediction includes three types of risk prediction: high-energy protons, low-energy particles, and high-energy electrons. The comprehensive risk real-time warning includes three types of risk warnings: SEU, surface charging, and deep charging, all of which are expressed by risk indices.

Table 1. Introduction to automatic data acquisition of multi-satellite space environmental risk prediction and real-time warning system.

Name	Level	Period	Source
High-energy proton flow data	L2	5 min	NCSW
High-energy electron flow data	L2	1 min	NCSW
Low-energy ion flow data	L2	1 min	NCSW
Low-energy electron flow data	L2	1 min	NCSW
Deep charge potential data	L2	5 min	NCSW
Surface differential potential data	L2	1 min	NCSW
Monitoring data of solar proton events	L2	1 d	NCSW
Ap index forecast data	/	1 d	NCSW
AE index forecast data	/	1 min	WDC Kyoto
Proton event probability data	/	1 min	SWPC
High-energy proton Fp value	/	1 d	SWPC
Solar wind	/	1 min	SWPC
Ap index	/	1 min	SWPC

2.1. High-Energy Proton Risk Prediction

The prediction probability of solar proton events is positively correlated with the flux of solar high-energy protons [30,31] (reference). This article uses the high-energy proton risk prediction at 02:00 UT every day based on the probability of solar proton events P1 published by NCSW on T + 0 day and the probability prediction of high-energy proton Fp value P2 based on SWPC, respectively, selecting the larger p value for level classification to predict the hourly high-energy proton risk level for FY-4A and FY-4B satellites in the next 24 h [32,33]. The risk level is set using the Chinese national industry standard solar proton event intensity classification [34] and combined with the author's satellite business operation experience, as shown in Table 2.

Table 2. Classification of high-energy proton risk levels.

Level	Solar Proton Event Probability	Risk
L1	$p < 30\%$	No
L2	$30\% \leq p < 60\%$	Medium
L3	$p \geq 60\%$	High

Based on engineering experience [35], when SWPC shows a high-energy proton flux Fp with energy greater than 10 MeV at 22:00 on T − 1, which is higher than 10 $cm^{-2}s^{-1}sr^{-1}$, the high-energy proton risk of the T + 0 satellite is directly labeled as Level 3.

2.2. Low-Energy Particle Risk Prediction

High-flux low-energy particles are the source of surface charging for satellites. This article is based on the geomagnetic AE index for hourly calculation, and the Ap index prediction results for daily calculation. By predicting the relevant geomagnetic disturbance indices (AE and Ap), the higher value of the two risk levels is adopted, achieving the prediction of low-energy particle risk [36–41].

The increase in geomagnetic AE index is positively correlated with the corresponding increase in local plasma, and is related to the local time of the satellite. This article adopts the author's early warning method for the surface charging effect of geosynchronous orbit satellites and the method patented by the early warning system [42]. The local time of the satellite's location is divided into four time domains, and the corresponding relationship between the AE index in each time domain and the surface charging potential is different. Among them, the safe period is from 6:00 to 21:00 local time at the Subsatellite Point (SSP), during which there will be no surface charging effect; i.e., the surface potential will always be 0.

SSP 21:00 LT–24:00 LT is transition zone I. Taking the AE time point as the satellite local time (TL), the calculated values of the surface charging potential model for the time period from TL − 1 to TL + 1 (time units in hours) are as follows:

$$U_1 = -40(AE - 150) \quad (1)$$

In Equation (1), AE is the latest hourly average of the AE index, in nT; U_1 calculates the surface charging potential in volts for the transition zone I mode.

SSP 0:00 LT–4:00 LT is the disturbance zone. Taking the AE time point as the satellite local time (TL), the calculated values of the surface charging potential model for the time period from TL − 1 to TL + 1 (time units in hours) are as follows:

$$U_2 = -50(AE - 100) \quad (2)$$

In Equation (2), AE is the latest hourly average of the AE index, in nT; U_2 calculates the surface charging potential in volts for the disturbance zone mode.

SSP 4:00 LT–6:00 LT is the transition zone II. Taking the AE time point as the satellite local time (TL), the calculated values of the surface charging potential model for the time period from TL − 1 to TL + 1 (time unit is hour) are as follows:

$$U_3 = -40(AE - 200) \quad (3)$$

In Equation (3), AE is the latest 1 h average of the AE index, in nT; U_3 calculates the surface charging potential in volts for the transition zone II mode.

Hourly risk prediction of low-energy particles is based on the surface charging potential calculation model provided by the surface charging detection results of Fengyun-4, where $U = U_1 \cup U_2 \cup U_3$, represents the time zone where different real-time satellite points are located. To adapt to the application of other satellites in geosynchronous orbit, the surface charging potential model calculation value U of AE index is used to classify the level of surface charging danger. The level setting is based on the author's long-term operational experience in satellite management, as expressed in Table 3.

Table 3. Risk level classification of low-energy particles I.

Level	Surface Charging Potential of FY-4 Satellite	Risk
L1	$U > -5000$ V	No
L2	$-10{,}000$ V $\leq U < -5000$ V	Medium
L3	$U \leq -10{,}000$ V	High

The daily prediction adopts the FY-4A and FY-4B satellite low-energy particle risk prediction daily products, with daily 01:00 UT analysis. The NCSW product Ap index prediction data are read for 24 h prediction value for risk assessment. The setting of surface charging hazard level is based on the author's engineering construction experience, as shown in Table 4.

Table 4. Risk level classification of low-energy particles II.

Level	Geomagnetic Ap Index	Risk
L1	Ap < 15	No
L2	15 ≤ Ap < 25	Medium
L3	Ap > 25	High

2.3. High-Energy Electron Risk Prediction

High-energy electron risk prediction obtains high-energy particle data, and performs prediction calculations and deep charge amplitude prediction calculations separately to determine the level of high-energy deep charge [43–47]. This article adopts the author's

patented method for predicting high-energy electron burst events [48] to achieve high-energy particle deep charge risk prediction.

The 2 MeV Daily high-energy particle risk prediction T + 0 daily E > 2 MeV high-energy electron daily flux is calculated using the following formula:

$$\lg(Ff) = -0.163 + 0.2877 \times 10{-}2\ V + 0.8233l\ g\ (F0) + 0.0177\ Ap \quad (4)$$

In Equation (4), V is the average speed of the solar wind on T − 1 day and is the high-energy electron flux on T = 1 day, and Ap is the SWPC on T − 1 day Ap index.

The daily high-energy particle risk prediction obtains the high-energy electron differential flux counting products of the FY-4A and FY-4B satellites on the T + 0 day, analyzes the daily integrated flux data of E > 2 MeV high-energy electron flux Ft at a sampling interval of 2 s on the T − 1 day, and accumulates it to double the calculation.

The high-energy electron risk forecast is launched once a day at 03:00 UT, and the deep charge level of high-energy particles can be determined by the high-energy electron flux of E > 2 MeV on that day. The risk level is determined using the Chinese meteorological industry standard electronic daily integral intensity grading with energy above 2 MeV at the geostationary orbit [49], and is set based on the author's engineering construction experience [50], as shown in Table 5.

Table 5. Classification of high-energy electronics risk levels.

Level	High-Energy Electron Flux	Risk
L1	$Ff \leq 109\ cm^{-2}d^{-1}sr^{-1}$	No
L2	$109\ cm^{-2}d^{-1}sr^{-1} < Ff \leq 3 \times 109\ cm^{-2}d^{-1}sr^{-1}$	Medium
L3	$Ff \geq 3 \times 109\ cm^{-2}d^{-1}sr^{-1}$	High

2.4. Real-Time Warning of Single-Event Upset Risk

The probability of single-event upset significantly increases in the process of higher strong proton events, mainly caused by high-energy protons with medium to high energy. The main characteristic parameter is the high-energy proton flux of 80–165 MeV [51,52]. Therefore, after obtaining the FY-4A and FY-4B satellite high-energy proton flux FP prediction data products, proton energy spectrum calculations are carried out. The real-time warning subsystem for single-event upset risk automatically analyzes high-energy proton flux data of 80–165 MeV, averages FP data over a 5 min period, calculates the probability of single-event upset, and statistically analyzes the corresponding relationship between high-energy proton flux and single particle event occurrence rate. The risk level setting for single-event upset is based on the author's engineering construction experience [53], as shown in Table 6.

Table 6. Classification of risk levels for single-event upset.

Level	High-Energy Proton Flux	Risk
L1	$Fp < 10\ cm^{-2}s^{-1}sr^{-1}$	No
L2	$10\ cm^{-2}s^{-1}sr^{-1} \leq Fp < 100\ cm^{-2}s^{-1}sr^{-1}$	Medium
L3	$Fp \geq 100\ cm^{-2}s^{-1}sr^{-1}$	High

2.5. Real-Time Warning of Surface Charging Risk

The subsatellite point of FY-4A and FY-4B satellites are different, and the risk of low-energy particles is different [54]. The real-time warning subsystem for surface charging risk in multi-satellite space environment obtains data from FY-4A and FY-4B satellite surface differential potential upward detection, automatically analyzes the differential potential value U of satellite upward surface potential probe C with a sampling interval of 2 s within 1 min at the latest time [55], judges the extra satellite and other ionospheric environments, and divides the levels of charging events for each satellite. Based on long-term operational

experience in satellite management, the author of this article sets the surface charging warning level recognition level, as shown in Table 7.

Table 7. Classification of surface charging risk levels.

Level	Different Surface Potential	Risk
L1	$U \geq -5000V$	No
L2	$-10{,}000\ V \leq U < -5000\ V$	Medium
L3	$U \leq -10{,}000\ V$	High

2.6. Real-Time Warning of Deep Charging Risk

The risk prediction of deep charging in multi-satellite space environment is initiated every 5 min to obtain the latest high-energy electron differential flux counts of FY-4A and FY-4B satellites, analyze the E > 2 MeV high-energy electron flux Ft data at a sampling interval of 2 s within 5 min [56], average the flux during this period, and obtain the net input charge of multi-satellite deep charging. By analyzing the corresponding relationship between the input charge and deep charging voltage, the deep charging warning level is determined, realizing real-time warning of deep charging [57,58]. The setting of the multi-star deep charging warning level is based on the author's engineering construction experience, as shown in Table 8.

Table 8. Classification of risk levels for deep charging.

Level	High-Energy Electron Flux	Risk
L1	$Ft < 8 \times 103\ cm^{-2}s^{-1}sr^{-1}$	No
L2	$8 \times 103\ cm^{-2}s^{-1}sr^{-1} \leq Ft < 1.5 \times 104\ cm^{-2}s^{-1}sr^{-1}$	Medium
L3	$Ft \geq 1.5 \times 104\ cm^{-2}s^{-1}sr^{-1}$	High

2.7. Comprehensive Risk Index Strategy

The multi-satellite space environment risk prediction and warning system needs to visually display the impact of the space environment on satellites. For various space weather factors, a comprehensive risk index is used to express the risk. Among them, high-energy protons, low-energy particles, and high-energy electrons are the three risk predictions, and single-event upset, surface charging, and deep charging are the three risk warnings. The highest one is selected as the comprehensive risk prediction level and the comprehensive risk real-time warning level. For the convenience of business personnel, the comprehensive risk index consists of risk levels and textual prompts. The first-level risk prompt is for safety, the second-level risk prompt is for attention, and the third-level risk prompt is for caution. The process of spatial environmental comprehensive risk index is shown in Figure 1. The comprehensive risk index guideline is shown in Tables 9 and 10.

Table 9. Multi-satellite space environmental risk prediction index guideline.

Risk Prediction Index			
	Level 1	Level 2	Level 3
High-Energy Proton Risk Warning	No	Medium	High
Low-Energy Particle Risk Warning	No	Medium	High
High-Energy Electron Risk Warning	No	Medium	High
Comprehensive Prediction Risk Level	L1	L2 as highest	L3 as highest
Comprehensive Prediction Risk Warning	Safe	Attention	Warning

Table 10. Multi-satellite space environmental risk real-time warning index guideline.

Risk Real-Time Warning Index			
	Level 1	Level 2	Level 3
Single-Event Upset Risk Warning	No	Medium	High
Surface Charging Risk Warning	No	Medium	High
Deep Charging Risk Warning	No	Medium	High
Comprehensive Warning Risk Level	L1	L2 as highest	L3 as highest
Comprehensive Risk Warning	Safe	Attention	Warning

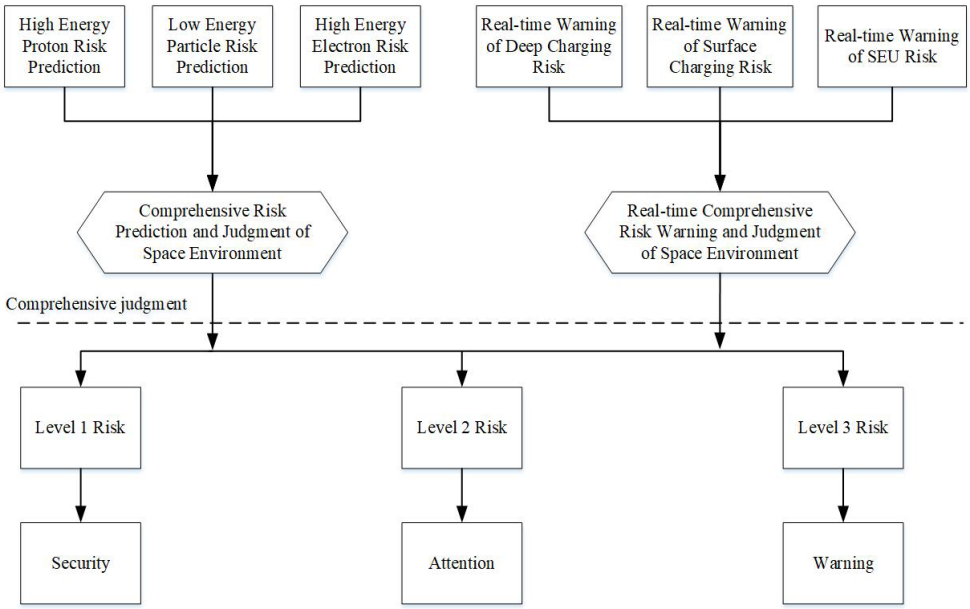


Figure 1. Flow chart of spatial environment comprehensive risk index.

3. Results and Discussion

3.1. System Deployment

The multi-satellite space environmental risk prediction and real-time warning system has achieved an intelligent space risk assessment for the safety of multiple stationary meteorological satellites for the first time, providing a reference basis for quickly locating the source of operational faults in satellite ground systems. The system was successfully deployed in the FY4-(02) batch of ground application systems in March 2023, with the main task of predicting and warning based on the spatial environment data of FY-4A and FY-4B satellites, providing auxiliary references for the safety and operation of multi-satellite satellites, and providing quantitative data and visualization services for intelligent, fully automated satellite ground integrated command and control, satellite safety management, satellite ground system business operation status monitoring, and multi-satellite command and control platforms. To ensure the high reliability and stability of the system, multi-source datasets and various hierarchical parameters are designed with the ability to adjust the configuration during business operation. To enhance the reuse rate of the system construction, the system adopts embedded design at both the data input interface and output end, which can provide hierarchical computation and data support for subsequent satellite security management and the iterative construction of space weather systems, as well as multiple types of user needs. The multi-satellite space environmental risk prediction and real-time warning system products are shown in Table 11.

The error between the predicted results of various risk indices and the measured data is less than one level; the high-energy proton risk prediction subsystem predicts the risk level of high-energy protons one day in advance to predict the next 24 h's risk; the low-energy particle risk prediction subsystem provides hourly prediction 3 h in advance and one-day prediction in the next 24 h; and the high-energy electron risk prediction subsystem

is for predicting one day in advance for the next 24 h. The system combines the above three predictions to generate risk index prediction products for each hour, with a prediction accuracy that is better than 80%. The real-time warning subsystem for the single-event upset risk divides the level of the single-event upset risk warning once every 5 min. The real-time warning subsystem for the surface charging risk divides the level of the surface charging risk warning once every 1 min. The real-time warning subsystem for the deep charging risk divides the level of the deep charging risk warning once every 5 min. The system generates risk index warning products minute by minute based on the above three types of warnings, and the warning accuracy is better than 90%. The system has the ability to access multiple online users simultaneously, and flexibly configure access permissions for different user levels. The forecast and warning information are stored in the information folder of the day. Local online storage shall not be less than 15 d, and the integrity of online storage shall be 100%. The data playback speed can be flexibly adjusted. The process of the multi-satellite space environmental risk prediction and real-time warning system is shown in Figure 2. The interface demonstration of the multi-satellite space environmental risk prediction and real-time warning system is shown in Figure 3.

Table 11. Multi-satellite space environmental risk prediction and real-time warning system products.

Name	Level	Format	Period	Release Time (UTC)	Content
High-energy proton risk prediction	L3	json	24 h	02:00	Prediction of T + 24 h High-Energy Proton Risk Level
Low-energy particle risk prediction	L3	json	1 h/24 h	hh:00/01:00	Prediction of T + 3 h/T + 24 h Low-Energy Particle Risk Level
High-energy electron risk prediction	L3	json	24 h	03:00	Prediction of T + 24 h High-Energy Electron Risk Level
Real-time warning of SEU	L3	json	5 min	Real-time	Real-time warning of SEU risk level
Real-time warning of surface charging risks	L3	json	1 min	Real-time	Real-time warning of surface charging risk level
Real-time warning of deep charging risks	L3	json	1 min	Real-time	Real-time warning of deep charging risk level
Comprehensive risk prediction	L3	json	1 h	hh:00	Prediction of comprehensive risk level
Comprehensive risk real-time warning	L3	json	1 min	Real-time	Real-time warning comprehensive risk level

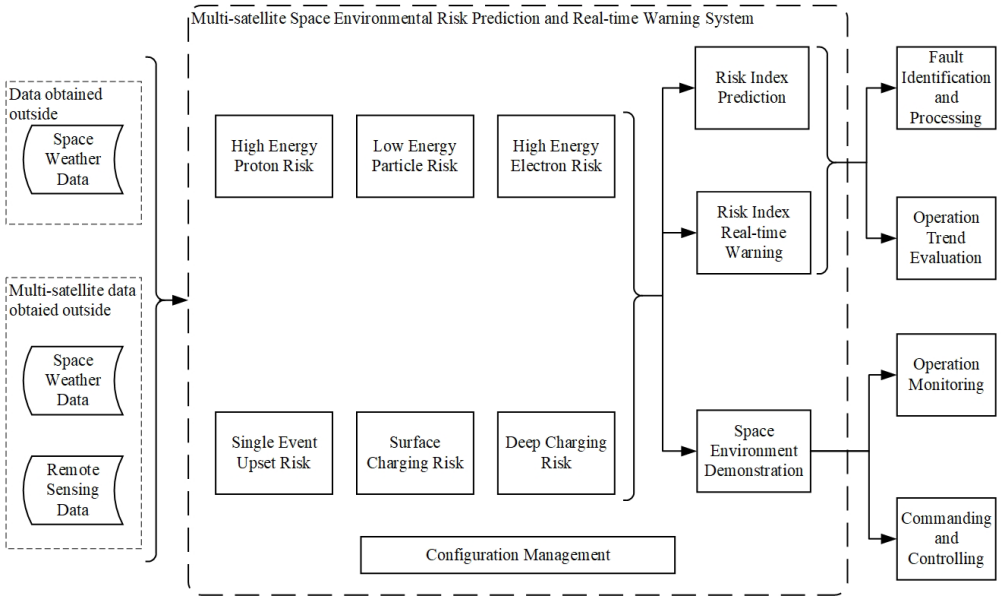


Figure 2. Flow chart of multi-satellite space environmental risk prediction and real-time warning system.



Figure 3. Demonstration of the interface for multi-satellite space environmental risk prediction and real-time warning system.

3.2. Case Studies

From the deployment of the system on 17 March 2023 to 30 June 2023, there were few factors affecting satellite safety due to space weather factors. On 21 April 2023, the high-energy particle environment was at the background level, with the high-energy proton flux greater than 10 MeV at 0.1 $cm^{-2}sr^{-1}s^{-1}$ and high-energy electron flux greater than 2 MeV at 108 $sr^{-1}d^{-1}$. As shown in Figure 4, the highest level of geomagnetic activity on that day was perturbation. Starting from 16:00 UT, the solar wind speed gradually increased from 360 km/s to 711 km/s at 22:00 UT. During the T1 period, the geomagnetic AE index continued to be maintained at 500–800 nT, indicating that plasma was injected from the magnetic tail, forming surface charging conditions. It is of great importance to note that the provisional and final AE indices are not available yet as the values are derived from unverified raw data, and the real-time AE indices can be seen from the website (https://wdc.kugi.kyoto-u.ac.jp/ae_realtime/202304/index_20230421.html, accessed on 14 April 2022). There should be a diagram showing the 24 h time evolution of FY-4A and FY4B spatial environmental forecasting and real-time warning risk levels on 21 April 2023, as shown in Figures 5–7. The risk level switch time is shown on Tables 12–14.

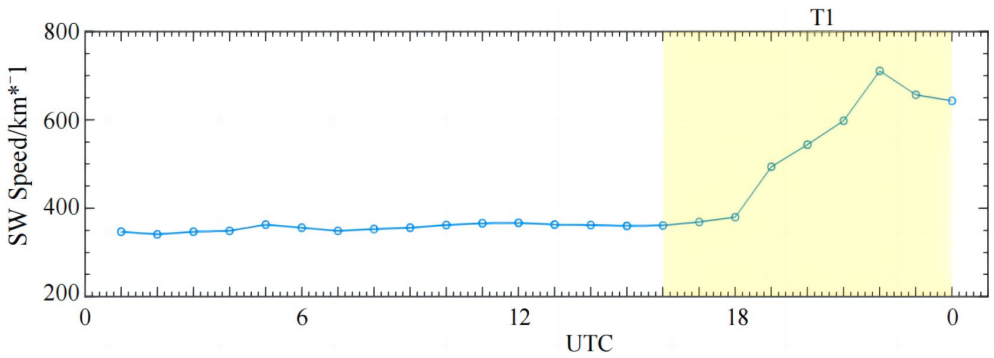


Figure 4. Variation of solar wind speed index during on 21 April 2023.

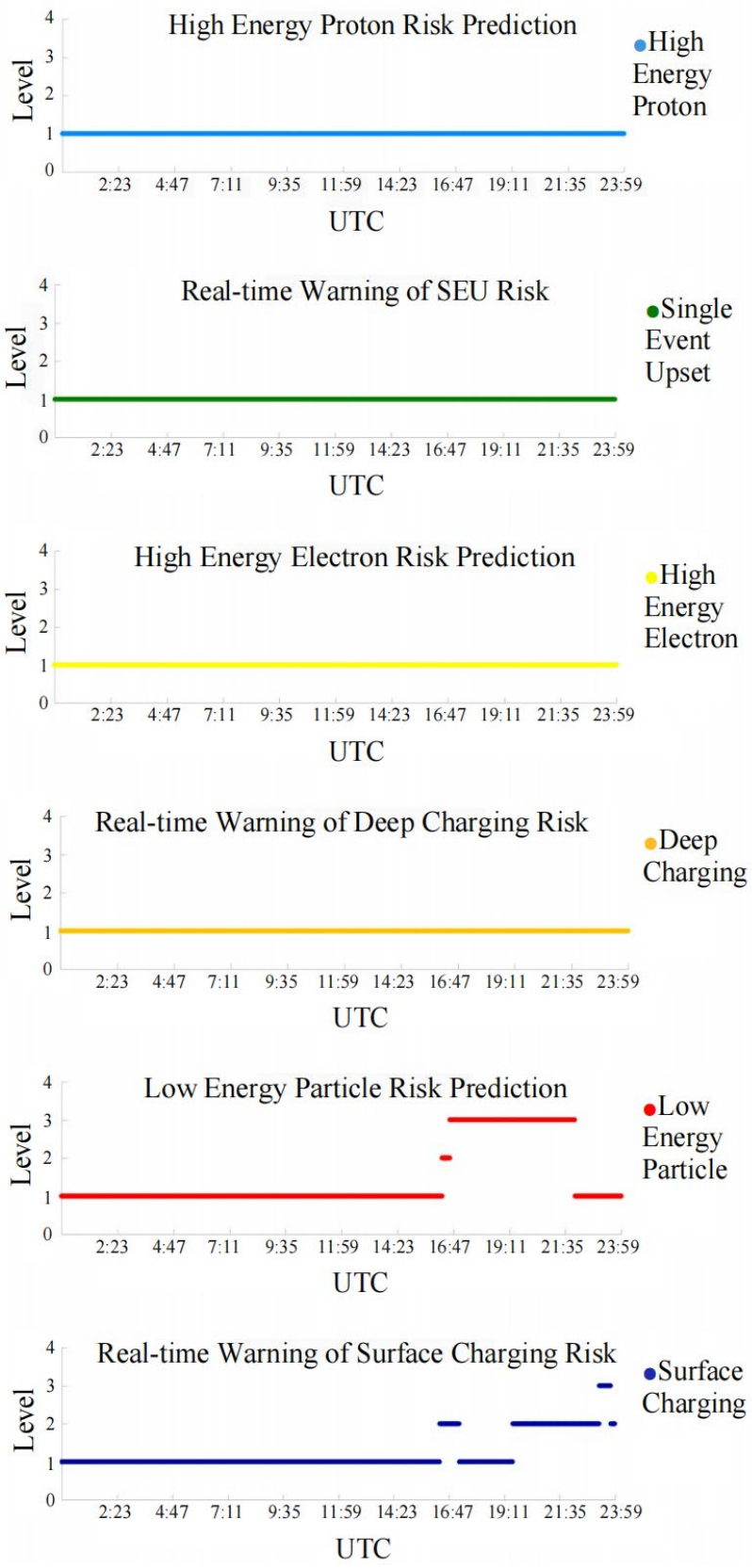


Figure 5. The 24 h time evolution of FY-4A space environment prediction and real-time warning risk level on 21 April 2023.

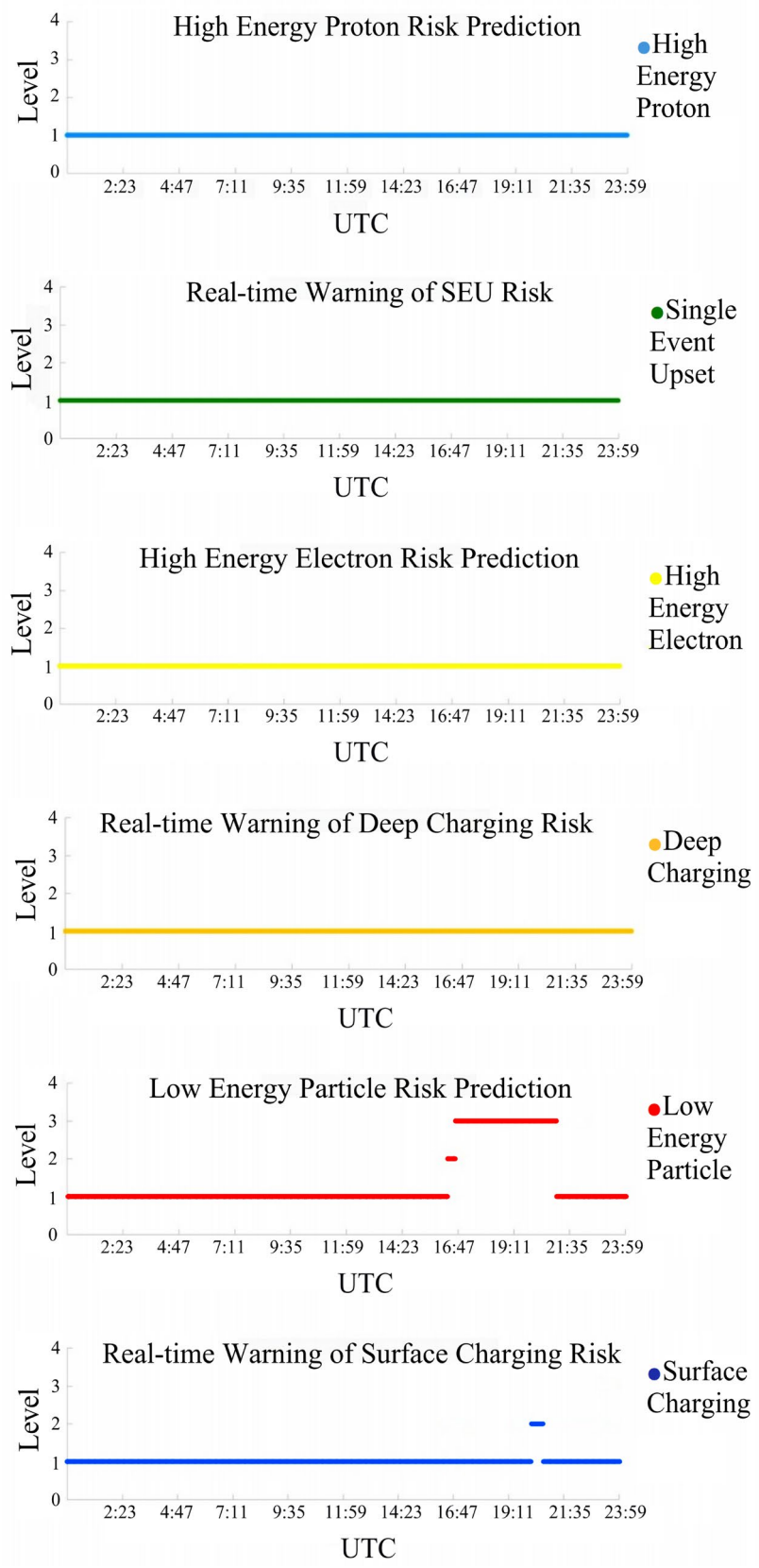


Figure 6. The 24 h time evolution of FY-4B space environment prediction and real-time warning risk level on 21 April 2023.

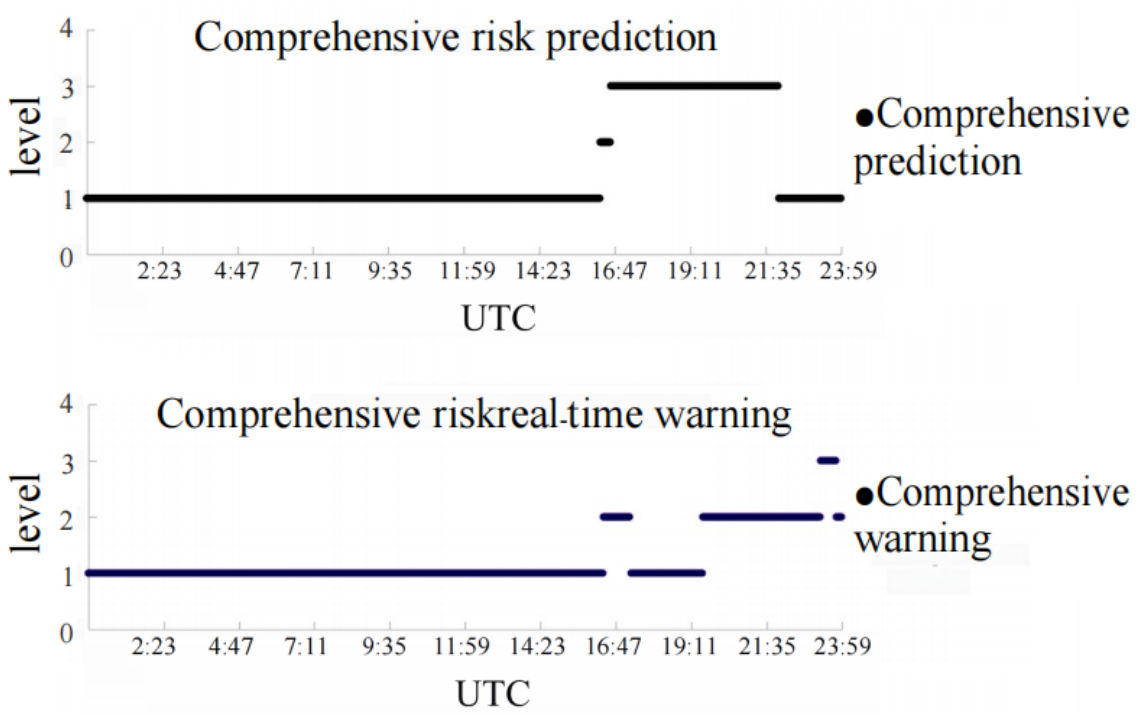


Figure 7. The 24 h time evolution of risk levels for comprehensive prediction and real-time warning of space environment on 21 April 2023.

Table 12. FY-4A space environment prediction and real-time warning risk level switch time on 21 April 2023.

Satellite	Elements	Start Time	End Time	Level
FY4A	High-Energy Proton	/	/	1
	SEU	/	/	1
	High-Energy Electron	/	/	1
	Deep Charging	/	/	1
	Low-Energy Particle	16:19	16:38	2
		16:39	22:08	3
	Surface Charging	16:24	17:19	2
		19:34	23:18	2
		23:19	23:48	3
		23:49	23:58	2

Table 13. FY-4B space environment prediction and real-time warning risk level switch time on 21 April 2023.

Satellite	Elements	Start Time	End Time	Level
FY4B	High-Energy Proton	/	/	1
	SEU	/	/	1
	High-Energy Electron	/	/	1
	Deep Charging	/	/	1
	Low-Energy Particle	16:19	16:38	2
		16:39	21:08	3
	Surface Charging	20:09	20:48	2

Table 14. Comprehensive risk index in the multi-satellite space environment switch time.

Type	Start Time	End Time	Level
Comprehensive Prediction	16:19	16:38	2
	16:39	22:08	3
Comprehensive Warning	16:24	17:19	2
	19:34	23:18	2
	23:19	23:48	3
	23:49	23:58	2

On 21 April 2023, geomagnetic disturbances triggered a plasma injection event in the magnetotail, which resulted in the formation of low-energy particle environmental conditions for surface charging during night measurements in the geostationary orbit. The multi-satellite space environmental risk prediction and warning system judged the entire day to be 24 h long, with FY-4A and FY-4B high-energy protons and low-energy particle risk prediction, as well as the real-time warning level for single-event upset and surface charging risks all at Level 1. Starting from 15:00 UT of the FY-4A satellite and 14:00 UT of the FY-4B satellite, the surface charging detectors carried by them gradually entered the shaded area, and the surface charging phenomenon began to appear. Among them, the C probe is facing upwards and in a completely dark state. The charging potential can reach a high level. As the charge accumulates on the probe surface, the potential detected by FY-4A tends to increase. FY-4B begins to weaken due to the low-energy particles in its position, and the surface charging effect weakens until it disappears after 21:00 UT. FY-4A low-energy particle risk prediction 16:19 UT–16:38 UT has a risk level of 2, 16:39 UT–22:08 UT has a risk level of 3, FY-4B low-energy particle risk prediction 16:19 UT–16:38 UT has a risk level of 2, 16:39 UT–21:08 UT has a risk level of 3, and other time periods have a risk level of 1; FY-4A surface charging real-time risk warning 16:24 UT–17:19 UT, 19:34 UT–23:18 UT, and 23:49 UT–23:58 UT have a risk level of 2, 23:19 UT–23:48 UT has a risk level of 3, FY-4B surface charging real-time risk warning 20:09 UT–20:48 UT has a risk level of 2, and other warning periods have a risk level of 1. The comprehensive forecast risk level is higher than the comprehensive warning risk level, and the overall time period difference between Level 2 and Level 3 risks is within 3 h, which is consistent with the design plan. The analysis of the surface charging process recorded by two satellites shows that the surface charging process is basically consistent, but, due to differences in the probe parameters, the potential size is inconsistent. When the low-energy particle environmental conditions required for surface charging occur, geostationary orbit satellites will experience the corresponding surface charging phenomena. On 21 April 2023, the surface differential charging potential changes of the A/B/C probes for the FY-4A and FY-4B satellite space weather loads are shown in Figures 8 and 9.

The FY-4A low-energy particle risk prediction for Level 3 has been delayed by 1 h compared to FY-4B, mainly due to the Earth's rotation. The FY-4B satellite located at E123.5° entered the area adjacent to the magnetic tail earlier than the FY-4A satellite located at E105°, thus entering the high-temperature plasma zone earlier and forming surface charging 1 h earlier. FY-4A has a real-time risk warning time of nearly 5 h longer than FY-4B for Level 2 and 3 of surface charging, which is related to the equipment used by two satellites to detect surface charging. FY-4A's surface charging detection equipment is more sensitive, making it easier to reach higher charging levels. The risk level of FY-4A and FY-4B low-energy particle risk prediction is higher than the real-time risk warning level of surface charging. This is because low-energy particles are the source of surface charging, and they need a certain accumulation time on the surface charging detector to form a certain surface potential.

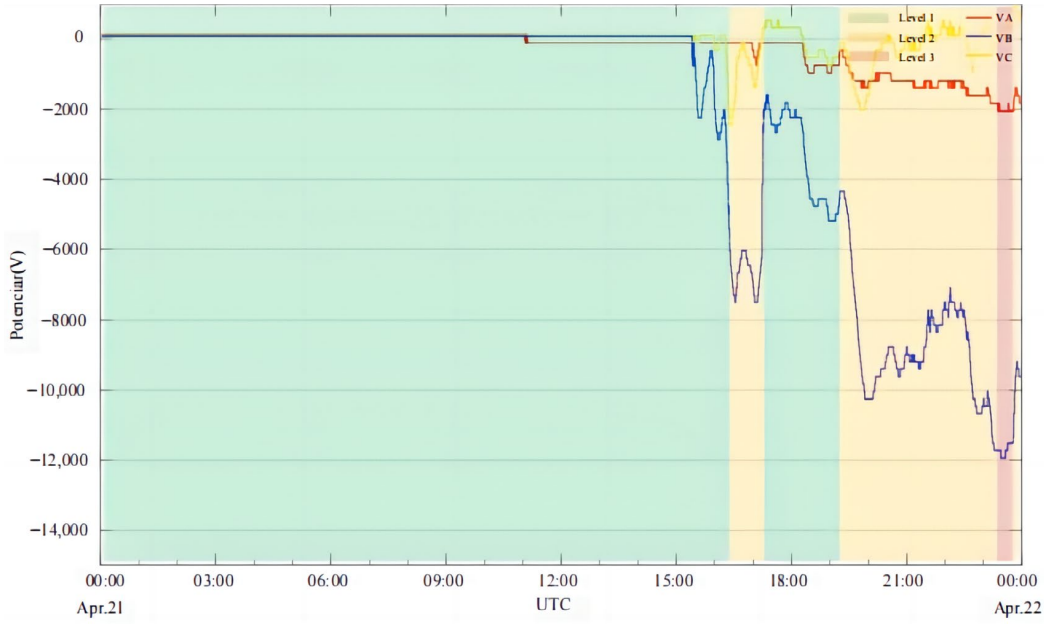


Figure 8. Changes in surface differential charging potential of three probes A/B/C for FY-4A satellite space weather load and surface charging real-time risk level switch on 21 April 2023.

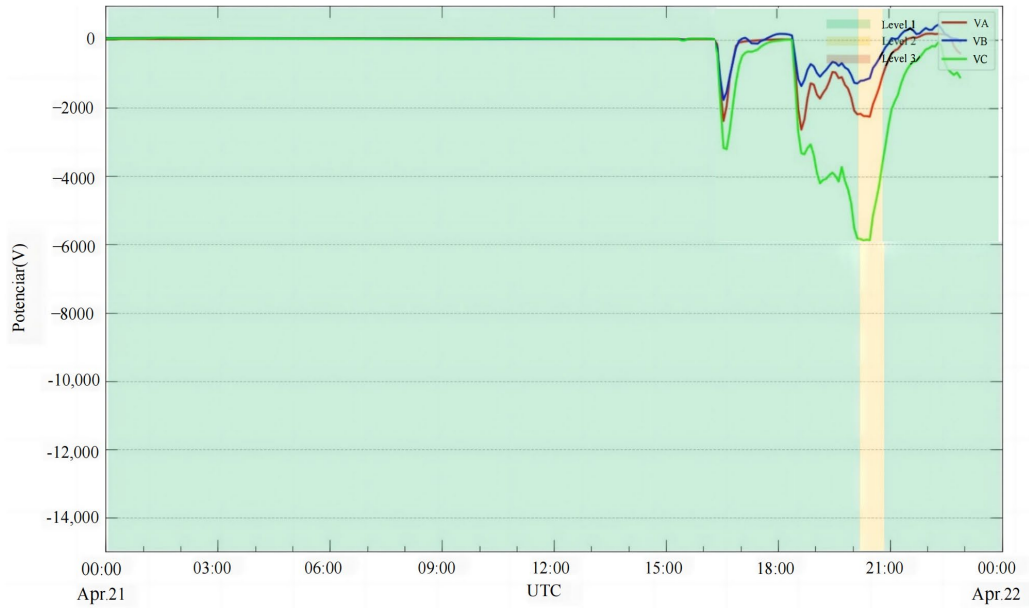


Figure 9. Changes in surface differential charging potential of three probes A/B/C for FY-4B satellite space weather load and surface charging real-time risk level switch on 21 April 2023.

On 21 April 2023, the surface differential charging potential changes of the A/B/C probes of the FY-4A and FY-4B satellite space weather loads were consistent with the temporal evolution of low-energy particle risk prediction and real-time risk warning risk levels for surface charging in the multi-satellite space environmental risk prediction and warning system. The satellite telemetry signal was stable on that day, and the satellite ground business was operating normally. There were no abnormal observation data caused by a single particle upset or abnormal alarm phenomenon of deep charging, which is consistent with the prediction and real-time warning results. This indicates that the design theory of the system is correct and feasible, and the timeliness during the operation is high, and the results are effective and reliable.

4. Conclusions

The multi-satellite space environmental risk prediction and early warning system is the first to address the safety of Fengyun-series high-orbit satellites in the face of complex spatial environmental factors. It is based on the FY-4A and FY-4B space weather detection results, NCSW prediction results, and some open-source data for the first time. It adopts Chinese national industry standards, Chinese meteorological industry standards, and invention patents, and combines the author's years of engineering practice and satellite safety management experience to focus on the high-energy protons of FY-4A and FY-4B satellites, low-energy particle and high-energy proton risk prediction, the real-time warning for a single-event upset, surface charging, and deep charging to design and deploy an automatic system. At present, the main construction of the system has been completed and business trial operation services have been provided to users. For the first time, an intelligent spatial risk assessment has been implemented for the safety of multiple stationary meteorological satellites, generating risk index prediction products hour by hour and risk index warning products minute by minute. The error between the predicted results of various risk indices and the measured data is less than one level, with a prediction accuracy that is better than 80% and a warning accuracy that is better than 90%. During the typical space weather event on 21 April 2023, the FY-4A and FY-4B low-energy particles were correctly predicted and warned about, as well as the high-risk level of surface charging. The verification results showed that the system design theory was correct, the system operation was stable, and the prediction and real-time warning results were effective and reliable. There are many factors that affect satellite safety in complex space weather environments, with a wide variety of satellite platforms and payload types. The successful deployment of this system can play an important data support role in the pre-deployment of satellite security management during the active period of the future space environment, in response to the requirements of satellite security management.

Space weather prediction and the early warning for the safety of spacecraft are a fundamental capability directly related to the survival and development of human beings in the space age. This paper only focuses on the prediction and early warning of various elements of the space environment for the safety of high-orbit meteorological satellites, and preliminarily establishes a set of operational systems. In the future, the system can rely on the integrated monitoring data of the "causal chain" in solar–terrestrial space and the panoramic view of the earth space to build an intelligent risk assessment system for regional spatial environmental disturbances and the effects of high- and low-orbit satellites, aircraft, navigation, communication, radar, power, and other facilities. With the continuous deepening of research on the basic physical processes that affect space weather changes, the construction of intelligent prediction and early warning systems with machine deep-learning capabilities, the development of a "full chain" system for space weather monitoring, research, modeling, and forecasting, and the establishment of globalized and standardized services for different spatial regions. It is an important trend for the future development of space weather prediction and early warning, which can provide useful references for the development of society in the space environment.

Author Contributions: Conceptualization, N.K. and B.X.; methodology, B.X., N.K. and W.Z.; investigation, W.Z.; validation, L.Z.; formal analysis, P.H. and J.Q.; resources, Y.Z.; visualization, C.Z.; funding acquisition, W.Z. and B.X. All authors have read and agreed to the published version of the manuscript.

Funding: This work is supported by the Key Laboratory of Space Weather, National Satellite Meteorological Center (National Center for Space Weather) the Chinese Merdian Project SK2023007.

Data Availability Statement: The original contributions presented in the study are included in the article, further inquiries can be directed to the corresponding author.

Acknowledgments: The authors would like to express his sincere gratitude to China Meteorological Administration 'Space Weather Monitoring and Alerting' Key Innovation Team (CMA2024ZD01) and 'Ionospheric Forecast and Alerting' Youth Innovation Team (CM MA2024QN09). In addition, the authors are grateful for the insight and help of the anonymous reviewers, as well as the selfless support and help of the relevant teachers and students of the Faculty of Geographical Sciences of Beijing Normal University. The multi-satellite space weather environment prediction and real-time warning index products are available from the FY4-(02) batch of the Ground Application System.

Conflicts of Interest: The authors declare no conflicts of interest.

References

1. Zhang, S.; Shi, C.; Shen, R.; Wu, J. Improved Assimilation of Fengyun-3 Satellite-Based Snow Cover Fraction in Northeastern China. *J. Meteorolog. Res.* **2019**, *33*, 960–975. [CrossRef]
2. Wang, C.; Chang, Z.; Zhang, X.; Shen, G.; Zhang, S.; Sun, Y.; Li, J.; Jing, T.; Zhang, H.; Sun, Y.; et al. Proton belt variations traced back to Fengyun-1C satellite observations. *Earth Planet. Phys.* **2020**, *4*, 611–618. [CrossRef]
3. Gusev, A.A.; Jayanthi, U.B.; Choque, K.T.; Pugacheva, G.I.; Schuch, N.; Spjeldvik, W.N. Antiproton radiation belt produced by cosmic rays in the Earth magnetosphere. *Geophys. Res. Lett.* **2003**, *30*, 10–14. [CrossRef]
4. Heckman, H.H.; Nakano, G.H. Low-altitude trapped protons during Solar Minimum Period, 1962–1966. *J. Geophys. Res.* **1969**, *74*, 3575–3590. [CrossRef]
5. Eastes, R.W.; McClintock, W.E.; Burns, A.G.; Anderson, D.N.; Andersson, L.; Aryal, S.; Budzien, S.A.; Cai, X.; Codrescu, M.; Correira, J.T.; et al. Initial observations by the GOLD mission. *J. Geophys. Res. Space Phys.* **2020**, *125*, e2020JA027823. [CrossRef]
6. Friis-Christensen, E.; Lühr, H.; Knudsen, D.; Haagmans, R. SWARM—An earth Observation Mission investigating Geospace. *Adv. Space Res.* **2008**, *41*, 210–216. [CrossRef]
7. Zhang, Z.; Lu, F.; Fang, X.; Tang, S.; Zhang, X.; Xu, Y.; Han, W.; Nie, S.; Shen, Y.; Zhou, Y. Application and Development of FY-4 Meteorological Satellite. *Aero Space Shanghai* **2017**, *34*, 8–19. [CrossRef]
8. Yang, Z.; Zhang, P.; Gu, S.; Zhu, A.; Hu, X.; Yang, J. Application and Development of FY-3 Meteorological Satellite. *Aero Space Shanghai* **2017**, *34*, 1–7. [CrossRef]
9. Jia, Y.; Ren, L.; Guo, Q. Techniques for Improving Precision in Fengyun-4 Meteorological Satellite Ranging System. *Meteorol. Sci. Technol.* **2020**, *48*, 630–634. [CrossRef]
10. Jia, Y.; Qiu, Y.; Guo, Q. Correction and Confirmation of Coordinate Measurement Points for FY-4 Ranging Stations. *Meteorol. Sci. Technol.* **2021**, *49*, 42–347. [CrossRef]
11. Kang, N.; Guo, Y.; Hui, W.; He, X.; Peng, Y. Single Event Upset Protection on FPGA Loaded in Lightning Mapping Imager of FY-4A Satellite. *Meteorol. Sci. Technol.* **2020**, *48*, 68–75. [CrossRef]
12. Yang, J.; Xian, D.; Tang, S.H. The latest developments and applications of Fengyun series meteorological satellite. *Spec. Rep.* **2018**, *11*, 8–14.
13. Huang, C.; Shi, H.; Gao, L.; Liu, M.; Chen, Q.; Fu, D.; Wang, S.; Yuan, Y.; Xia, X. Fengyun-4 Geostationary Satellite-Based Solar Energy Nowcasting System and Its Application in North China. *Adv. Atmos. Sci.* **2022**, *39*, 1316–1328. [CrossRef]
14. Gubby, R.; Evans, J. Space Environment Effects and Satellite Design. *J. Atmos. Sol.-Terr. Phys.* **2002**, *64*, 1723–1733. [CrossRef]
15. Randall, C.E. Stratospheric Effects of Energetic Particle Precipitation in 2003–2004. *Geophys. Res. Lett.* **2005**, *37*, 223–249. [CrossRef]
16. Rozanov, E.; Callis, L.; Schlesinger, M.; Yang, F.; Andronova, N.; Zubov, V. Atmospheric Response to NOy Source due to Energetic Electron Precipitation. *Geophys. Res. Lett.* **2005**, *32*, 65–82. [CrossRef]
17. Fennell, J.F.; Roeder, J.L.; Berg, G.A.; Elsen, R.K. HEO Satellite Frame and Differential Charging and SCATHA Low-Level Frame Charging. *IEEE Trans. Plasma Sci.* **2008**, *36*, 2271–2279. [CrossRef]
18. Reames, D.V. The Two Sources of Solar Energetic Particles. *Space Sci. Rev.* **2013**, *175*, 53–92. [CrossRef]
19. Dröge, W.; Kartavykh, Y.Y.; Dresing, N.; Heber, B.; Klassen, A. Wide Longitudinal Distribution of Interplanetary Electrons Following the 7 February 2010 Solar Event: Observations and Transport modeling. *J. Geophys. Res. Space Phys.* **2015**, *119*, 257–273. [CrossRef]
20. Verkhoglyadova, O.P.; Li, G.; Ao, X.; Zank, G.P. Radial Dependence of Peak Proton and Iron Ion Fluxes in Solar Energetic Particle Events: Application of the Path Code. *Astrophys. J.* **2012**, *757*, 667–672. [CrossRef]
21. Wang, Y.; Qin, G. Estimation of the release time of solar energetic particles near the Sun. *Astrophys. J.* **2015**, *79*, 111–112. [CrossRef]
22. Lu, N.; Ding, L.; Zheng, X.; Ye, X.; Li, C.; Lyu, D.; Zhang, P.; Hu, X.; Zhou, C.; You, Z.; et al. Introduction of the radiometric benchmark satellite being developed in China for remote sensing. *J. Remote Sens.* **2020**, *24*, 672–680. [CrossRef]
23. Wu, D.; Wang, K.; Ye, X.; Wang, Y.; Fang, W. Space Cryogenic Absolute Radiometer. *Chin. J. Lumin.* **2019**, *40*, 1015–1021. [CrossRef]
24. Dong, Y. Consideration on the Development of Fengyun Series Satellite System. *Aero Space Shanghai* **2021**, *38*, 76–84. [CrossRef]
25. Chen, Q.; Chen, X.; Wang, Z. Intelligent Observation Requirements and Visions for Meteorological Satellite. *Aero Space Shanghai* **2020**, *29*, 17–22.
26. Zhang, P.; Yang, J.; Guan, M.; Xu, Z.; Wang, J. WMO Space Program and Internationalization of Fengyun Meteorological Satellites. *Adv. Meteorol. Sci. Technol.* **2022**, *12*, 56–63. [CrossRef]

27. Lu, F.; Zhang, X.; Chen, B.; Liu, H.; Wu, R.; Han, Q.; Feng, X.; Li, Y.; Zhang, Z. Imaging characteristics and application prospects of Fengyun-4 meteorological satellite. *J. Shandong. Meteorol.* **2017**, *37*, 12.
28. Bain, H.M.; Steenburgh, R.A.; Onsager, T.G.; Stitely, E.M. A Summary of NOAA Space Weather Prediction Center Proton Event Forecast Performance and Skill. *Space Weather* **2021**, *47*, 379–382. [CrossRef]
29. Yamazaki, Y.; Yumoto, K.; Uozumi, T.; Abe, S.; Cardinal, M.G.; McNamara, D.; Marshall, R.; Shevtsov, B.M.; Solovyev, S.I. Reexamination of the S_q-EEJ Relationship Based on Extended Magnetometer Networks in the East Asian Region. *J. Geophys. Res. Space Phys.* **2010**, *115*, 342–358. [CrossRef]
30. Evans, D.; Garrett, H.; Jun, I.; Evans, R.; Chow, J. Long-term Observations of the Trapped High-energy Proton Population (L < 4) by the NOAA Polar Orbiting Environmental Satellites (POES). *Adv. Space Res.* **2008**, *41*, 1261–1268. [CrossRef]
31. Li, G.; Shalchi, A.; Ao, X.; Zank, G.; Verkhoglyadova, O. Particle Acceleration and Transport at an Oblique CME-driven Shock. *Adv. Space Res.* **2012**, *49*, 1067–1075. [CrossRef]
32. Barnard, L.A.; de Koning, C.A.; Scott, C.J.; Owens, M.J.; Wilkinson, J.; Davies, J.A. Testing the Current Paradigm for Space Weather Prediction with Heliospheric Imagers. *Space Weather* **2017**, *15*, 74–88. [CrossRef]
33. Crown, M.D. Validation of the NOAA Space Weather Prediction Center's Solar Flare Forecasting Look-up Table and Forecaster-issued Probabilities. *Space Weather. Int. J. Res. Appl.* **2016**, *10*, 38–48. [CrossRef]
34. *GB/T 31161-2014*; Intensity Classification of Solar Proton Events. China Meteorological Administration: Beijing, China, 2014.
35. Xue, B. The application of spectrum of energetic protons accelerated by CME in the geomagnetic storm forecast. *J. Geophys. Eng.* **2012**, *55*, 738–743. [CrossRef]
36. Hu, J.; Li, G.; Fu, S.; Zank, G.; Ao, X. Modeling a Single SEP Event from Multiple Vantage Points Using the iPATH Model. *Astrophys. J. Lett.* **2018**, *854*, 191–195. [CrossRef]
37. Hu, J.; Li, G.; Ao, X.; Zank, G.P.; Verkhoglyadova, O. Modeling Particle Acceleration and Transport at a 2-D CME-Driven Shock. *J. Geophys. Res. A. Space Phys.* **2017**, *122*, 10938–10963. [CrossRef]
38. Balch, C.C. Updated Verification of the Space Weather Prediction Center's Solar Energetic Particle Prediction Model. *Space Weather* **2008**, *7*, 176–188. [CrossRef]
39. Kuznetsov, S.N.; Myagkova, I.N. Energetic Trapped Proton and Electron Flux Variations at Low Altitudes Measured Onboard CORONAS-I Satellite, Their Connection with the Particle Flux Variations in Geotationary Orbit. *Adv. Space Res.* **2002**, *30*, 2319–2323. [CrossRef]
40. Li, Y.; Feng, Y.; Zhang, S.; Liu, S.; Zhang, J.; Wei, G. The study of geomagnetic jerk from 2010 to 2021 based on hourly mean data from global geomagnetic observatories. *Earth Planet. Phys.* **2023**, *7*, 39–48. [CrossRef]
41. Rich, F.J.; Bono, J.M.; Burke, W.J.; Gentile, L.C. A space-based proxy for the Dst index. *J. Geophys. Res.* **2007**, *112*, 521–537. [CrossRef]
42. Key Laboratory of Space Weather, National Satellite Meteorological Center (National Center for Space Weather). Early Warning Methods and Systems for Surface Charging Effects of Geosynchronous Orbit Satellites. China Patent CN111703593A, 17 August 2021.
43. Kaplan, M.; Hudaverdi, M. The correlations of space weather and satellite anomalies: RASAT. In Proceedings of the 2013 6th International Conference on Recent Advances in Space Technologies (RAST), Istanbul, Turkey, 12–14 June 2013; Volume 32, pp. 1377–1394. [CrossRef]
44. Kurazhkovskaya, N.A.; Klain, B.I. The Effect of Interruption of "Serpentine Emission" (SE) in the Polar Cap during Geomagnetic Storm Sudden Commencements (SSC). *Geomagn. Aeron.* **2022**, *62*, 573–581. [CrossRef]
45. Biktash, L.Z. Evolution of Dst index, cosmic rays and global temperature during solar cycles 20–23. *Adv. Space Res.* **2014**, *33*, 269–280. [CrossRef]
46. Temerin, M.; Li, X. The Dst Index Underestimates the Solar Cycle Variation of Geomagnetic Activity. *J. Geophys. Res. Space Phys.* **2015**, *120*, 5603–5607. [CrossRef] [PubMed]
47. Banerjee, A.; Bej, A.; Chatterjee, T.N. On the Existence of a Long Range Correlation in the Geomagnetic Disturbance Storm Time (Dst) Index. *Astrophys. Space Sci.* **2011**, *337*, 23–32. [CrossRef]
48. Key Laboratory of Space Weather, National Satellite Meteorological Center (National Center for Space Weather). Method, Device and Storage Medium and Device for Predicting High-Energy Lectron Burst Events. China Patent CN110231643A, 14 August 2020.
49. *QX/T 367-2016*; Classification of Daily Integrated Intensity of Electrons with Energy above 2 MeV in Geostationary Orbits. China Meteorological Press: Beijing, China, 2016.
50. Guo, C.; Xue, B.; Lin, Z. Approach for Predicting the Energetic Electron Flux in Geosynchronous Earth Orbit. *Chin. J. Space Sci.* **2013**, *33*, 9–13. [CrossRef]
51. Noeldeke, C.; Boettcher, M.; Mohr, U.; Gaisser, S.; Rua, M.A.; Eickhoff, J.; Leslie, M.; Von Thun, M.; Klinkner, S.; Varatharajoo, R. Flight Single Event Upset Investigations on the "Flying Laptop" Satellite Mission. *Adv. Space Res.* **2020**, *67*, 232–238. [CrossRef]
52. Cui, X.; Liu, L. Mitigating single event upset of FPGA for the onboard bus control of satellite. *Microelectron. Reliab.* **2020**, *114*, 113–120. [CrossRef]
53. Zhang, X.; Liu, S.; Wu, Y. Statistical Analysis of Space Weather Effects on Satellites Anomalies. *Chin. J. Space Sci.* **2015**, *35*, 461–472. [CrossRef]
54. Spencer, E.; Srinivas, P.; Vadepu, S.K. Global Energy Dynamics During Substorms on 9 March 2008 and 26 February 2008 Using Satellite Observations and the WINDMI Model. *J. Geophys. Res. Space Phys.* **2019**, *124*, 1698–1710. [CrossRef]

55. Cao, X.; Ma, X.; Zhang, X.; Chen, A.; Dong, J.; Ni, B.; Dou, X.; Wang, X. Cross-satellite calibration of high-energy electron fluxes measured by FengYun-4A based on Arase observations. *Earth Planet. Phys.* **2023**, *7*, 565–575. [CrossRef]
56. Molinie, P.; Dessante, P.; Hanna, R.; Paulmier, T.; Dirassen, B.; Belhaj, M.; Payan, D.; Balcon, N. Polyimide and FEP Charging Behavior under Multienergetic Electron-beam Irradiation. *IEEE Trans. Dielectr. Electr. Insul.* **2012**, *19*, 398–412. [CrossRef]
57. Key Laboratory of Space Weather, National Satellite Meteorological Center (National Center for Space Weather). A Risk Assessment and Monitoring Method for Deep Charging of Internal Media in Satellites, China. China Patent CN114399221A, 26 April 2022.
58. Li, C.; Chen, D. Deep charging effect risk model assessment based on Bayesian methods. *Chin. J. Geophys.* **2019**, *62*, 1991–2000. (In Chinese)

Disclaimer/Publisher's Note: The statements, opinions and data contained in all publications are solely those of the individual author(s) and contributor(s) and not of MDPI and/or the editor(s). MDPI and/or the editor(s) disclaim responsibility for any injury to people or property resulting from any ideas, methods, instructions or products referred to in the content.